3D Printing by Selective Laser Sintering (SLS)

Luis Carrillo, Michael McMahon, Michael Rogatinsky, Daniel Valledor

Dept. of Electrical and Computer Engineering,

University of Central Florida, Orlando, Florida, 32816-2450, USA

***Abstract* — This paper describes the general design decisions and methods used for the development of a functional SLS 3D printer as well as all custom components used therein. Both components and testing fall into 4 general categories: (1) The mechanical design, which includes the device structure as well as the electromechanical components like linear actuators; (2) The electrical systems, broken into power control and processing; (3) The software/computer systems, comprised of a microcontroller and firmware as well as a host server; (4) The Laser and laser safety system, including a diode laser and lens assembly along with cooling and eye protection.**

***Index Terms* — Selective Laser Sintering, Laser, Laser Printer, Additive Manufacturing.**

I. Introduction

Additive manufacturing (AM) [1] is a group of processes which enables three-dimensional construction of computer-aided design (CAD) models. These processes are often collectively known as 3D printing. 3D printing has seen adaptations in many industries, such as automotive part manufacturing [2], 3D printed scaffolding for tissue growth [3], prosthetic manufacturing [4], and more. This is not surprising; AM technologies boast higher degrees of freedom in the design space, a faster production time from virtual conception to manufactured parts, and a more environmentally friendly footprint, all at a more affordable cost [5]. While these technologies have many benefits and bring great capabilities to large businesses, the consumer and hobbyist market has struggled with introducing low-cost, easy-to-use printers. Two types of printers dominate the hobbyist market, and these printers have drawbacks that could be removed with the introduction of a different type of 3D printing technology: selective laser sintering (SLS). SLS printing has not reached a hobbyist or consumer market due to its high price. The most affordable SLS printer costs $5000 and comes as a kit, while the second most affordable option is $17,000. For the introduction of SLS printers to a consumer market to be successful, the printer must be affordable, safe, and feature similar print specifications as already existing technologies.

3D printing comes in many flavors. One subset of 3D printing focuses on material extrusion. In this type of AM, a material is gathered and fed through a nozzle. The nozzle changes the material in a way such that it can be deposited in a different physical state. For example, fused deposition modeling (FDM) [6] uses a spool of thermoplastic filament. The filament runs through the nozzle, is heated to a temperature just below its melting point, and then the nozzle is guided in a 2D plane. As the nozzle moves along the 2D plane, the filament is pushed through the nozzle, and patterns are formed. Once a layer has been formed, the nozzle moves upwards and repeats the process. In this manner, a 3D object can be created.

FDM is the most common hobbyist 3D printer. It is easy to use, is not extraordinarily expensive, yet still has excellent printing capabilities. Another type of printing, stereolithography (SLA) [7], uses light exposure to induce chemical and physical changes in a light-sensitive polymer. SLA is the second most common hobbyist 3D printer. Between FDM and SLA, there are few other types of AM technologies available at the consumer or hobbyist level.

Another type of 3D printing, called powder bed fusion [8], enables 3D construction through the use of a bed of powder. This type of printing differs greatly from FDM printing. The nozzle no longer feeds state-altered material in a 2D plane. Instead, a laser focuses onto a 2D sheet of powdered material. The thermal energy from the laser induces physical changes in the powdered material. These physical changes either melt or sinter the powdered material together. To transition from a 2D plane to a 3D object, there exist different methods, but most commonly the bed of powder is first lowered some height z. Once the bed lowers by $-z$, another bed adjacent to the build area rises by $+z$. Then, some mechanism pushes the powder from the $+z$ plate to the $-z$ plate, covering the original build plate with a layer of powder with a thickness of z. Then, the exposure process begins, and the plate movements repeat.

These powder bed 3D printing processes can be categorized based on the type of thermal energy incident on the powder bed, as well as the powder bed material. Selective laser melting (SLM) uses a laser to melt powdered metal. The powder usually has a mean particle size of 50 μm ± 20 μm, although nanoparticle SLM is an area of active research. There also exists electron-beam melting (EBM),

where an electron beam acts as the source of thermal energy. There is also selective heat sintering (SHS), where a stream of hot air is used as the thermal energy. Selective laser sintering is another type of powder bed AM. It differs from SLM in that the thermal energy incident on the powder bed is not enough to induce a full state change from solid to liquid. Instead, the delivered thermal energy is tuned to specifically melt only the outside region of each particle, just enough to fuse or sinter them together, but not enough to fully melt the particle and cause reflow.

Powder bed printing methods offer great advantages over the most common printers found in the hobbyist communities, which are FDM and SLA printers. In FDM printing, the nozzle extrudes thermoplastic filament in a 2D plane. The nozzle then rises in the *z* direction which defines a new 2D plane. Material extrusion in the new 2D plane is restricted to areas that were printed in the prior layer. The nozzle cannot extrude filament in an area where there is nothing to support the extruded filament. This means overhanging structures in a CAD model must be accounted for during the initial design. Proper supports must be designed beforehand. CAD models with overhanging flat faces must have their faces beveled or curved such that there is sufficient support from the layers beneath to extrude material in the upper layers. In SLS, the need for support is completely eliminated. The 2D plane which supports building is always covered in powder, and as the build plate lowers, the unsintered powder supports the layers above it. This means each layer is self-supporting. Further, because each layer is self-supporting, the SLS process can use more of the 3D build volume than FDM or SLA by embedding multiple CAD models within the 3D volume. For example, to make many coffee mugs with FDM, the user is limited to the size of the 2D plane where the bottom supporting layer is defined. In SLS, the user can stack a large amount of coffee mugs within the build volume because there is no universal bottom supporting layer. Any layer can be the origin layer of a CAD model in SLS.

In this work, an affordable SLS printer was developed and tested to meet the demands of a growing hobbyist market. A mechanical assembly was created to deliver powder to a print bed. A robust software suite was integrated into the system to generate g-code and control the components of the printer, such as motors and laser. A power system was developed and created to provide stable power delivery from a wall adapter to the different components. Finally, a laser module was created which acts as the heat source for the sintering process

II. Printer Specifications

To build an SLS printer suitable for the hobbyist market, a budget of $600 was implemented. This is competitive with modern FDM and SLA printers, which are usually less than $1000 for high-quality printers. The print bed features an area of 100 cm^2, 10 cm in length on each side. The actual build area is an inset of the print bed to a space of 81 cm^2, or 9 cm long on each side. The print height is 9 cm tall, for an effective build volume of 729 cm^3. The printer receives all of its power from a North American standard wall outlet of 120 volts AC, and converters step down the voltage to the individual components as needed. G-code and other options are accessible to the user from a local host server. The motors controlling the moving parts of the printer have a minimum torque of 42.5 N·cm. The laser module features a laser diode operating at 447 nm with a maximum output power of 5 W. The focal length of the shape-corrected beam is 75 mm with a working distance of 68 mm. The spot size of the focused beam at the working distance is 200 μm. A track system scans along the *x* and *y* directions with a minimum speed of 30 $mm \cdot s^{-1}$. The material type usable with this printer is typical of SLS printers and includes thermoplastics, polyamides, thermoplastic elastomers (TPEs), and thermoplastic polyurethane (TPU). Additionally, this printer has the capability of sintering sugar-based compounds.

III. Mechanical System

The SLS 3D printer is comprised of four mechanical systems. The first system is the XY Track subassembly. The XY Track is responsible for moving the laser module in a cartesian plane. The second system is the powder reservoir. The powder reservoir houses the powder that will be used during the sintering process. The third system is the print bed reservoir. It houses the print during the sintering process. Lastly, the fourth system is the sweeper mechanism. The sweeper mechanism pushes the powder from the powder reservoir into the build reservoir after every sintered layer. A conceptual drawing of the mechanical system is shown in Fig.1. The final design of the mechanical system is shown in Fig. 2.

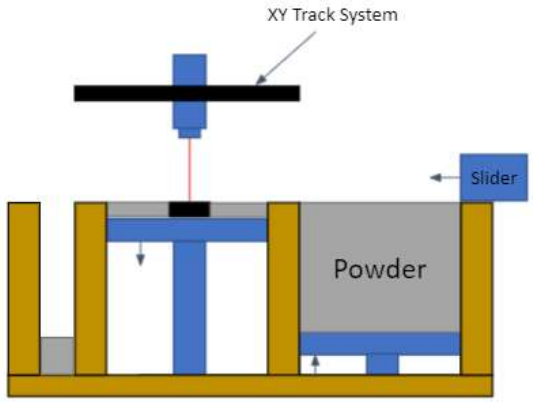

Fig. 1. Conceptual Drawing of Mechanical System

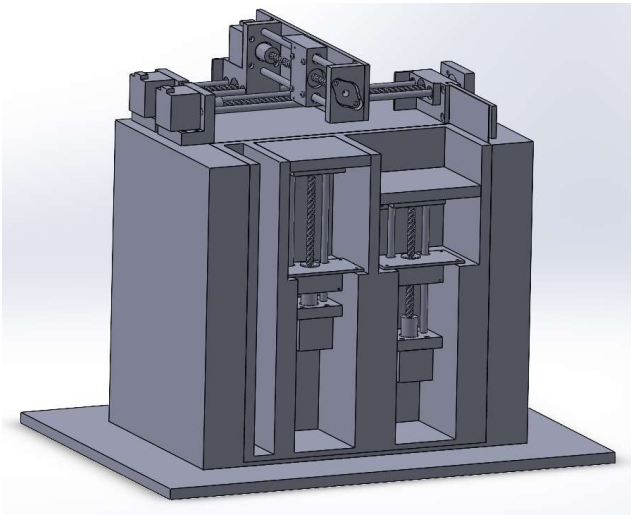

Fig. 2. The figure shows the 3D model of the final SLS printer design. Note: A side access panel covers the reservoirs in order to contain the powder, it is not shown in the figure.

A. Actuators

The foundation of motion within the SLS 3D printer is the linear actuator design. The linear actuator design is based off of a lead screw drive concept. The lead screw is attached to a motor via a coupler. As the motor turns, a flanged nut will move linearly on the screw. Guide rods are used to support the moving base along the linear path. The lead screw design is applied to all moving systems. The systems include the X-Y Track, Sweeper, Build Plate, and Powder Plate.

The lead screw chosen for the project has a 2 mm pitch and 4 starts. In order to calculate the lead, which is the linear displacement after one full rotation, we multiply the pitch and the number of starts. The lead for the chosen lead screw is 8 mm. The stepper motor chosen for the project is a standard NEMA 17 stepper motor. According to the data sheet, 200 full steps are equivalent to one rotation. Therefore, 25 full steps are needed to move one millimeter with our lead screw design. As described in the firmware section, steps per millimeter is an important value to ensure proper printer functionality.

Each actuator has a bump switch attached for calibration. When the bump switch is activated, we are able to establish the zero position. The bump switch is imperative for linear actuator control.

IV. Electrical System

The electrical module of the project is comprised of 4 submodules: Power, Computing, Laser Driver, and Motor Driver.

A. Power Supply

The Power submodule is composed out of a step-down 60Hz transformer, rectifier full-bridge and capacitor, five 9V regulators, one 5V regulator, and one 6V regulator with a 25us soft-start. A 60Hz transformer was chosen in order to simplify design, reduce cost, and because its weight and size do not affect the overall structure of the printer

The transformer has two possible step-down voltage ratios: 115:8 and 115:16. After AC/DC conversion, the stepped-down voltage would be 10.7V and 22.5V for each ratio. Considering the chip used for the 9V regulators has a dropout voltage of roughly 1.25V to .9V at 1A load current, we would be close to the output voltage of the AC/DC converter design with the lower step-down ratio. This would put us at risk of falling below the minimum input voltage for the 9V regulators. Thus, we design our regulators around an expected input voltage of 22.5V. This input voltage produces the following theoretical efficiencies at the expected load currents.

TABLE I
Regulator Efficiencies Across Expected Input Voltages

	9V Regulator at 0.7A Load		
Vin	18V	21V	24V
Efficiency	89.2%	88.9%	88.7%
	5V Regulator at 1A Load		
Vin	18V	21V	24V
Efficiency	89.2%	88.9%	88.7%
	6V Regulator at 3A Load		
Vin	18V	21V	24V
Efficiency	89.2%	88.9%	88.7%

The 9V regulators will be used to power all five stepper motors that draw maximum of about 0.7A or 6.3W each. From the 5V regulator we expect less than an 1A of current, so 5W or less. Lastly, our 6V regulator will deliver 3A to the laser adding another 18W to our total load. This adds up to a total of 54.5W delivered. However, having our efficiencies in mind we should expect a consumption of about 63W. This sets the theoretical efficiency of the entire power module to 86.5%. Lower real efficiencies will not affect the functioning of the module as long as we stay under the rated wattage of the transformer, 80W. Thus, real efficiencies need to stay above 68% to stay within the 80W limit.

B. MCU

The next part of the electrical module is the computing submodule. This includes the microcontroller chip along with all the external components required for it to function. The microcontroller would be used to control the 5 stepper motor drivers, the laser driver, and to communicate via USB to the computer graphic user interface. The chip used was the ATmega2560. Reasons for selecting this chip include its compatibility with existing 3D printing firmware, integrated memory, and number of digital pins. As for the external needs of the chip we have a 16MHz crystal oscillator, and given that the chip communicates with serial UART, we need to add a USB to UART bridge that will allow us to communicate with a computer via USB. The CP2102 was used for this bridge. Circuit details will be described further in the PCB section.

C. Stepper Motor Driver

The motors chosen for the project are NEMA 17 stepper motors. Unlike DC motors, stepper motors need a driver circuit in order to operate. A stepper motor is built up of coils that alternate in polarity in order to move the shaft. The switching in polarity must be properly timed for smooth operation. The base of the stepper motor driver circuit is the DRV8825 stepper motor driver integrated circuit (IC). The DRV8825 is controlled by a step/direction interface. The step/direction interface takes a square wave and a logic high/low signal to control the speed and direction of the motor, respectively. The rising edge of the square wave moves the stepper motor one step. Therefore, the frequency of the square wave determines the speed at which the motor turns. The direction of the spin is determined by a logic high/low signal. For instance, a logic high direction signal indicates to the motor to spin clockwise.

One of the capabilities of the DRV8825 is micro stepping. Micro stepping is a way to create fractional steps in between one full step. High micro stepping results in smoother motor operation compared to full steps. The DRV8825 is capable of reaching 1/32 micro stepping which is enabled in the stepper motor driver design. The DRV8825 also has a maximum current drive of 2.5 A. The NEMA 17 stepper motors are rated for 1.5 A therefore the drive is capable of delivering the necessary current requirements. The data sheet provides a full-scale current equation in order to set the maximum current.

$$I_{FS} = \frac{VREF}{A_v * R_{sense}} \quad . \qquad (1)$$

The data sheet states that the gaın, A_v, ıs equal to 5. The sense resistor value used in the design is 100 mOhms. Therefore, in order to set the full-scale current to 1.5 A, the reference voltage must be 0.75 V. Due to variances in resistor values, a trim potentiometer is used in the design as a voltage divider. The trim potentiometer allows the user to tune the reference voltage after fabrication and ensures a percise reference voltage.The operating supply voltage range is 8.2V to 45V. For the design and throughout testing, the supply voltage used was 9V.

D. Laser Driver

The purpose of a laser driver circuit is to control the output power of a laser diode. The main requirements for the laser driver circuit are a soft start DC voltage, a constant current source, and a method to control the output power. The base of the laser driver design is a voltage-to-current source. The design consists of an operational amplifier, a sense resistor, and a power MOSFET. The operational amplifier acts as a unity gain buffer with the amplifier output attached to the gate of the MOSFET and the feedback attached to the source of the MOSFET. The laser diode is connected to the drain and the sense resistor is connected to the source. The fundamental schematic of the circuit is shown in Fig. 3.

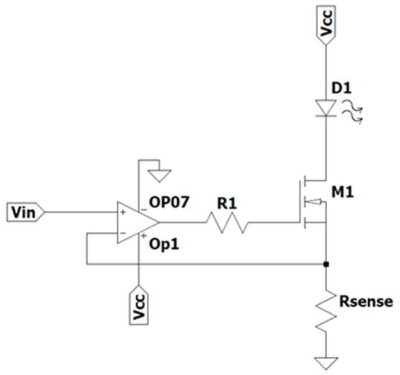

Fig. 3. The foundation of the laser driver circuit is shown above. The design is based off a voltage-to-current converter.

The current across the diode is equal to the current across the resistor which is set by Vin. Therefore, the diode current is equal to Vin divided by the sense resistor. According to the laser diode data sheet, 3 A is needed to achieve the full output power of 5W. In order to control the laser power with the firmware, a digital potentiometer is used as a voltage divider for Vin. The digital potentiometer uses SPI communication to set the potentiometer wiper. The design uses a 0.4 Ohm sense resistor so the voltage range for Vin is 0 – 1.2 V with respect to the maximum current of 3 A.

The laser driver uses a supply voltage of 6 V, and the chosen voltage regulator has a built-in soft start. Laser diodes are sensitive to current spikes and ESD. The purpose of the soft start is to ensure there are no current spikes upon laser turn-on. The 6V regulator is designed to have a soft start of 25 us.

V. Firmware

In this section, the firmware will be discussed as well as some broader design choices regarding the processing needs of the project. This can be broken down into firmware, hardware, and server/graphical host.

The Firmware for this project was built with the opensource Repetier firmware as a base and modified to support the needs of an SLS printer. This helps to ensure that the expected functionality of the printer, namely the Gcode parsing as well as the movement scheduling works as expected by the slicer to produce a correct print, while also allowing the customizability to add in the needed functionality like custom Gcode operations for the sweeper mechanism and build reservoir. It also makes it easy to make modifications where needed for minor changes like controlling the laser driver with a digital potentiometer (via spi signaling) instead of the standard PWM signal.

In order to run the firmware, an appropriate microcontroller needed to be chosen. Initially we intended to use the RP2040 MCU from Raspberry Pi, but we later found that the Atmel Atmega2560 was a better choice due to support with our firmware. The 2040, while faster, cheaper, and generally better in every way used a different ISA then the 2560, and also had significantly fewer pins; these differences would require a significant overhaul to the code base in order to account for to use that particular chip.

Finally, in order to use the printer, the Repetier host software must be installed on the computer allowing the printer to be plugged in and used like any other office printer. There is of course the caveat that most programs don't support printing in 3d, but any that do and support Repetier's coms standard can connect and print just like an HP or Dell printer. The Host server also provides an interface to the printer which can be used to directly print supported files, view print status's and test/troubleshoot issues.

VI. Laser Module

The laser module design focused on delivering a clean spot shape and size of 200 μm at a distance of 67.5 mm from the end of the laser module to the powder bed. A blue laser diode was chosen as the light source due to its ease of use, weight, and size when compared to carbon dioxide lasers. The Osram PLPT9 450 LB_E has a central wavelength of 447 nm at 25℃ and a maximum output power of 5 watts, which fit the desired specifications.

Laser diodes are inherently astigmatic, so one objective of the laser module was to fix the astigmatism. The diode has divergence angles of 49° and 9° along the fast and slow axes respectively. Numerous methods exist to fix astigmatic beams [1], such as an anamorphic prism pair, cylindrical lens pair, or fiber coupling. An anamorphic prism pair has the disadvantage of displacing the optical axis, making module design more difficult. However, the prism pair is very tolerant to misalignment. Fiber coupling produces a clean beam with only minimal power loss but aligning fiber optics with 3D printed parts is not reliable. Cylindrical lens pairs are sensitive to misalignment but are easily mountable and maintain a common optical axis with the laser diode. For this reason, a cylindrical lens pair was chosen for astigmatism correction.

A cylindrical lens pair was selected such that the ratio of the focal lengths of the lenses was as close as possible to the ratio of the fast and slow divergence angles. The two cylindrical lenses have focal lengths of 3.91 mm and 22.19 mm for the slow and fast axes. The ratio of the diode divergences is 5.44 while the ratio of the selected lenses is 5.67. If these values were equal, the beam would be completely circular. To determine the resulting astigmatism, the beam size at the focusing lens was calculated to be 3.564 mm along the fast axis and 3.493 mm along the slow axis. This resulted in an eccentricity of 0.02 which is highly circular. Thus, the astigmatism was corrected.

With the size of the beam at the focusing lens determined, the distance to the required spot size could be calculated. The diffraction limited spot size was found to be 12 μm, which is well below the desired spot size. The spot size of 200 μm was found to be located at a distance of 67.6 mm using a 75 mm focal length focusing lens. This falls within the prescribed working distance and will fit nicely within the x-y scanning track.

The housing for the diode and the lenses must satisfy three conditions: 1), the laser diode housed within the heatsink must be cooled adequately; 2), the housing should

protect the lenses from debris and not disturb the powder bed below; 3), the housing should hold the lenses permanently and with near perfect alignment. The first condition was satisfied by ensuring air could flow sufficiently around the copper heatsink. 10 air channels were designed within the copper heatsink housing to drive air around the heatsink. A 60 mm 9 V fan was attached at the top of the module to force air into the module and around the copper housing. This satisfied the first condition. The second condition was satisfied by ensuring the laser module was enclosed entirely. Slits along the sides of the laser module direct air away from the bottom of the laser module. Had air been directed through the module to the bottom, it could exit near the focusing lens and disturb the powder below. This satisfied the second condition. To ensure an exact fit for the cylindrical and spherical lenses, a 3D printer was used to print mounts while performing a parameter sweep. This resulted in an array of mounts with internal diameters 25 microns different per iteration. This ensured the tolerances of the lenses, which were ±100 microns, could be handled appropriately. Once the proper size mounts were selected, they were translated along grooves in an optical tube to their best locations and glued in place, satisfying the third condition.

Because the first cylindrical had an effective focal length of almost 1 mm, the lens had to be placed nearly on the diode itself. Still, the divergent fast axis exited the cylindrical lens along the edges of the lens, resulting in spherical aberration. This spherical aberration severely affected the spot size. Attempts to block the spherical aberrations with an aperture stop were successful and the spot size returned to an acceptable size.

VI. PCB Design and Assembly

In this section the main design considerations will be discussed. All four electrical submodules were developed into PCBs, each with different aspects of layout to keep in mind depending on its application.

In the power module we will have traces carrying significantly high currents, therefore, to ensure we do not loose voltage to trace impedances, we need to make traces as wide as possible. This means using polygons instead of lines when possible. In addition to reducing trace impedance, polygons also improve temperature performance. As far as component placing, input capacitors and output inductors were places as close as possible to the regulator's input and switching pins respectively.

Moving on to the microcontroller module, the main concern in the design is at the USB to UART bridge connections. The standard micro-USB port carries the data in two different lines. One carries the inverse of the other. This allows the USB-UART bridge to look at the difference between the lines instead of their absolute values, making them less prone to noise errors. However, this creates the need of tracing these data lines D+ and D- as a differential pair with 90ohm impedance between them across the entirety of the trace. Easiest way to achieve this is by placing the bridge chip as close as possible to the USB port.

For the other electrical submodules, the considerations are the same as power, just ensuring that power traces are wide enough.

With the PCBs designed and manufactured, the next step is assembly. In order to reduce cost, which is one of the main objectives of the project, and because of component shortages, we decided to assemble the PCB in the Senior Design Lab. This was done using a stencil, solder paste, preheating bed, and hot air. This was only possible because parts were purposely chosen to be big enough to assemble with the tools available.

Lastly, heatsinks and fans were added to protect the parts from overheating. After stress test we can confirmed that all PCBs work as intended for long periods of time.

VI. Results

A. Line Test

One of the important components of our printer (or any printer) is consistency. In order to measure how well our printer could translate distances from Gcode into real movements, we devised a test to draw a series of 10mm and 100mm lines on the X and Y axes so as to measure the variation and identify possible causes to be fixed. The shape tested was modeled after a snake form the old game Snake™ in order to efficiently compress all of the needed tests and data into a shape that could fit into a single layer of the print bed and takes the shape of a snake making its way horizontally across the area while moving down one row with each pass. As the build area is 100x100 mm, this yields 10 100mm lines, and 10 10mm lines which can be measured and averaged to find the printers overall consistency. The drawing, shown in Fig. 4, displays the aforementioned snake pattern as well as the sum of all 10mm lines drawn on the y axes showing perfect consistency within our ability to measure. As seen in Table. II & III, the x axis seems to draw nearly perfect lines with a 0.46% error, however on closer inspection all lines with poor values are shown while the print head is moving in the negative x direction; that fact along with the consistent corner chamfer pattern seem to indicate that the issue lies in the friction between the pen and paper dragging the paper slightly from it not being fixed in place well enough. It can

therefore be concluded that while the measured error is within spec, the actual error would be far less provided an appropriate means were available to measure it.

Fig. 4. Line Test

XY Scanning Speed Test

The scanning speed of the XY track system was tested by attaching a pen to the base of the system and drawing the future laser path on a paper. The test model shown in Fig. 5(a) was generated in SolidWorks. The g code used for the test was generated using a slicer software called Cura. The g code was loaded into the Repetier software and the print was initiated. The goal of the test was to capture the actual scanning speed of the XY track system and compare the results to the designed model. The test ran until the midpoint of the second layer. The test was recorded with a camera and the video of the moving XY track system was used to analyze the scanning speed. The section of the video where the outer diameter of the figure was scanned was used to calculate the scanning speed. The measured diameter of the outer circle was 29 mm and the circumference was 91.106 mm. The segment of the video where the complete outer circle was scanned took frames. Using 30 frames per second, the duration was 2.2s. By taking the circumference and dividing by the duration, the measured scanning speed is then equal to 41.41 mm/s. The resulting value passes our scanning speed requirement. The scanned image result shown in Fig. 5(b) shows the accuracy of the scanning system. It is important to note that the pen was unable to retract. During the print, the laser module will turn on during the actual scanning and turn off during travel movements.

TABLE II
LINE TEST MEASUREMENTS

X	Y
100	10
100	10
100	10
98.9	10
100	10
98.5	10
100	10
99.1	10
100	10
98.9	10

TABLE III
LINE TEST STATISTICS

	X	Y
Avg	99.54	10
Std	0.58	0
Skew	-0.58957	-
Kurtosis	-1.50932	-

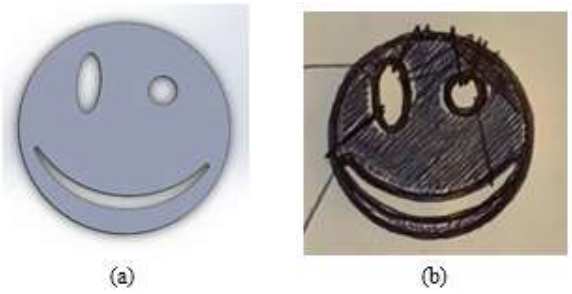

Fig. 5. (a) Test Model generated in SolidWorks. (b) Results of XY Scanning Speed Test.

VII. Conclusion

In this paper, we discussed the potential of SLS to enter the hobbyist market for AM at a competitive price. The design covered proves that replacing galvanometers with a X-Y scanning system can significantly reduce price while maintaining high printing quality. Thus, we are confident that SLS machines can be mass-produced at the cost of FDM or SLA printers of similar performance. Additionally, the SLS benefits of self-supporting property and wide material compatibility call for further research and development of this technology in order to make it the market leading 3D printer at the hobbyist level.

BIOGRAPHY

Michael Rogatinsky is a Senior at the University of Central Florida and is pursuing a Bachelor of Science in Computer Engineering this May. Michael is currently employed at MoxyTech, a Michigan based startup, and plans to continue working there for the foreseeable future. The possibility of working toward a masters or doctorate is also being considered, though Michael does not have any immediate plans in that regard.

Daniel Valledor is a senior at the University of Central Florida and plans on receiving his Bachelor of Science in Electrical Engineering in May 2022. Daniel currently works as a Systems Engineer in the College Work Experience Program (CWEP) with Lockheed Martin. He plans on pursuing a career at Lockheed Martin and a Masters.

Luis Carrillo is a senior student at the University of Central Florida and will be receiving his Bachelor of Science in Electrical Engineering in May 2022. Luis plans to pursue a Master of Science of Electrical Engineering at University of Central Florida after completing a summer internship with Texas Instruments Inc as a Validation Engineer.

Michael McMahon is a senior at the University of Central Florida in CREOL, the college of optics and photonics. Upon graduating in May 2022 with his Bachelor of Science in Photonic Science and Engineering, Michael will continue his graduate research in Dr. Stephen Kuebler's Nanophotonic Materials group where he is currently investigating optical metamaterials and their fabrication methods.

References

[1] I. Gibson, D.W. Rosen, B. Stucker, and M. Khorasani, *Additive Manufacturing Technologies*. Cham, Switzerland: Springer, 2010.

[2] R. Leal, F. M. Barreiros, L. Alves, F. Romeiro, J. C. Vasco, M. Santos, and C. Marto, "Additive manufacturing tooling for the automotive industry," *The International Journal of Advanced Manufacturing Technology*, vol. 92, no. 5-8, pp. 1671–1676, 2017.

[3] L. Diaz-Gomez, M. E. Elizondo, G. L. Koons, M. Diba, L. K. Chim, E. Cosgriff-Hernandez, A. J. Melchiorri, and A. G. Mikos, "Fiber engraving for bioink bioprinting within 3D printed tissue engineering scaffolds," *Bioprinting*, vol. 18, 2020.

[4] Y. Wang, Q. Tan, F. Pu, D. Boone, and M. Zhang, "A review of the application of additive manufacturing in Prosthetic and Orthotic Clinics from a biomechanical perspective," *Engineering*, vol. 6, no. 11, pp. 1258–1266, 2020.

[5] M. Attaran, "The rise of 3-D printing: The advantages of additive manufacturing over traditional manufacturing," *Business Horizons*, vol. 60, no. 5, pp. 677–688, 2017.

[6] P. Siemiński, "Introduction to fused deposition modeling," *Additive Manufacturing*, pp. 217–275, 2021.

[7] C. Schmidleithner and D. M. Kalaskar, "Stereolithography," *3D Printing*, 2018.

[8] S. Sun, M. Brandt, and M. Easton, "Powder Bed Fusion Processes," *Laser Additive Manufacturing*, pp. 55–77, 2017.